NeuroImage: Clinical 21 (2019) 101526

Contents lists available at ScienceDirect

NeuroImage: Clinical

journal homepage: www.elsevier.com/locate/ynicl

Bilateral functional connectivity at rest predicts apraxic symptoms after left hemisphere stroke

Christine E. Watson[a,1], Stephen J. Gotts[b,1], Alex Martin[b], Laurel J. Buxbaum[a,*]

[a] Moss Rehabilitation Research Institute, Elkins Park, PA 19027, USA
[b] Laboratory of Brain and Cognition, National Institute of Mental Health, NIH, Bethesda, MD 20892, USA

ARTICLE INFO

Keywords:
Apraxia
Praxis
Functional connectivity
Left hemisphere stroke
Action

ABSTRACT

Increasing evidence indicates that focal lesions following stroke cause alterations in connectivity among functional brain networks. Functional connectivity between hemispheres has been shown to be particularly critical for predicting stroke-related behavioral deficits and recovery of motor function and attention. Much less is known, however, about the relevance of interhemispheric functional connectivity for cognitive abilities like praxis that rely on strongly lateralized brain networks. In the current study, we examine correlations between symptoms of apraxia—a disorder of skilled action that cannot be attributed to lower-level sensory or motor impairments—and spontaneous, resting brain activity in functional MRI in chronic left hemisphere stroke patients and neurologically-intact control participants. Using a data-driven approach, we identified 32 regions-of-interest in which pairwise functional connectivity correlated with two distinct measures of apraxia, even when controlling for age, head motion, lesion volume, and other artifacts: overall ability to pantomime the typical *use* of a tool, and disproportionate difficulty pantomiming the use of tools associated with different, competing *use* and *grasp-to-move* actions (e.g., setting a kitchen timer versus picking it up). Better performance on both measures correlated with stronger interhemispheric functional connectivity. Relevant regions in the right hemisphere were often homologous to left hemisphere areas associated with tool use and action. Additionally, relative to overall pantomime accuracy, disproportionate difficulty pantomiming the use of tools associated with competing use and grasp actions was associated with weakened functional connectivity among a more strongly left-lateralized and peri-Sylvian set of brain regions. Finally, patient performance on both measures of apraxia was best predicted by a model that incorporated information about lesion location and functional connectivity, and functional connectivity continued to explain unique variance in behavior even after accounting for lesion loci. These results indicate that interhemispheric functional connectivity is relevant even for a strongly lateralized cognitive ability like praxis and emphasize the importance of the right hemisphere in skilled action.

1. Introduction

Limb apraxia, a disorder of skilled action not attributable to lower-level sensory or motor impairments, arises after left hemisphere lesions in the vast majority of cases (e.g., Haaland et al., 2000) and is apparent even in the ipsilesional left hand (e.g., Buxbaum et al., 2003). Meta-analyses of neuroimaging studies similarly reveal that a strongly left-lateralized functional network underlies skilled tool use, including left inferior and superior parietal lobes, posterior middle temporal gyrus (pMTG), posterior medial fusiform gyrus, lateral occipitotemporal cortex, inferior frontal gyrus (IFG), and dorsal and ventral premotor cortex (Lewis, 2006; Ishibashi et al., 2016). Yet, many individual neuroimaging studies of tool use additionally find (often weaker) activation in homologous right hemisphere regions (e.g., Hermsdörfer et al., 2007; Vingerhoets et al., 2011; Vry et al., 2015). Apraxia has also been reported after right hemisphere lesions (e.g., Haaland and Flaherty, 1984), but its occurrence is less frequent and deficits are typically relatively mild (Hanna-Pladdy et al., 2001; Stamenova et al., 2010) and sometimes less diverse (i.e., affecting imitation rather than tool use or pantomime, Barbieri and De Renzi, 1988, but see Hanna-Pladdy et al., 2001; Heath et al., 2001; Stamenova et al., 2010). To date, the contribution of the right hemisphere to typical praxis remains an unresolved question.

Lesion-based studies of apraxia, including those that use voxel-based lesion-symptom mapping (VLSM), correlate behavioral deficits with structural damage (e.g., Randerath et al., 2010; Buxbaum et al.,

* Corresponding author at: 50 Township Line Rd., Elkins Park, PA 19027, USA.
E-mail addresses: watsonch@einstein.edu (C.E. Watson), lbuxbaum@einstein.edu (L.J. Buxbaum).
[1] These authors contributed equally.

https://doi.org/10.1016/j.nicl.2018.08.033
Received 8 March 2018; Received in revised form 22 June 2018; Accepted 31 August 2018
Available online 31 August 2018

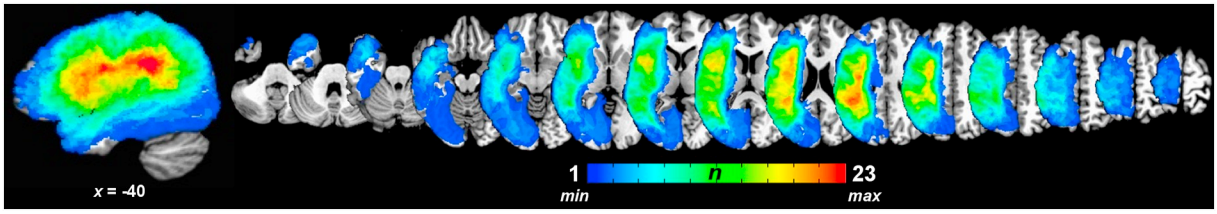

Fig. 1. Spatial distribution of left hemisphere lesions. All patient lesions (n = 35) displayed on the Colin27 template in Talairach-Tournoux standardized space (AFNI's TT_N27 template). Color bar represents the number of patients with lesions at a particular voxel.

2014) but are unable to assess the impact of left hemisphere stroke on right hemisphere regions that may also participate in skilled action. However, recent developments in neuroimaging methods for understanding the dynamics of brain networks (e.g., Bullmore and Sporns, 2009) enable investigation of the status of functional networks in both hemispheres after left hemisphere stroke. Studies of connectivity using temporal correlations between very slow fluctuations of brain activity at rest in functional MRI (rs-fMRI) (see Fox and Raichle, 2007; Power et al., 2014 for reviews) are particularly well-suited to clinical populations given the minimal demands during scanning (Fox and Greicius, 2010; Carter et al., 2012b; Ovadia-Caro et al., 2014; Siegel et al., 2017).

In the current study, we used rs-fMRI to examine the functional networks that underlie impaired praxis in chronic left hemisphere stroke. Participants who had experienced a left cerebrovascular accident pantomimed the use of familiar tools, and we assessed the relationship between behavioral performance and measures of functional connectivity. While tool use pantomime correlates with actual tool use (Jarry et al., 2013), it is not constrained by object structure (see Buxbaum et al., 2005a) and is more likely to reveal subtle deficits (Buxbaum et al., 2005b). We examined two distinct measures of praxis: overall accuracy, and a measure sensitive to impairments in resolving competition between actions. This second measure is calculated as disproportionate difficulty pantomiming the typical *use* of tools associated with different actions for *grasping-to-move* (e.g., setting a kitchen timer, picking it up) versus tools associated with the same typical actions for both using and grasping (e.g., picking up a coffee mug to move it or drink from it) (Jax and Buxbaum, 2010, 2013) and appears to index impairments of action selection and the resolution of competition between different possible actions (Watson and Buxbaum, 2015; Kalénine et al., 2016; Wamain et al., 2018). While impaired overall accuracy on the pantomime task is associated with lesions to the entire tool use network (e.g., Buxbaum et al., 2014; Hoeren et al., 2014), disproportionate difficulty with “conflict tools” versus “non-conflict tools” is associated with lesions to a peri-Sylvian subset of this network, namely, the left supramarginal gyrus (SMG), IFG, and anterior insula (Watson and Buxbaum, 2015). Using a data-driven, whole-brain approach (Gotts et al., 2012; Berman et al., 2016), we predicted that impaired tool use pantomime would correlate with disrupted functional connectivity between left hemisphere regions that support tool use (Lewis, 2006; Ishibashi et al., 2016). Further, we expected that disproportionate difficulty with conflict tools would correlate with connectivity specifically between left SMG and IFG/anterior insula (Watson and Buxbaum, 2015).

A number of recent rs-fMRI studies suggest that the status of interhemispheric functional connectivity following stroke is critical for predicting behavioral deficits and recovery in the domains of motor function and attention—cognitive abilities supported by bilateral brain networks (He et al., 2007; Carter et al., 2010; Carter et al., 2012a; Baldassarre et al., 2014; Urbin et al., 2014; Xu et al., 2014). An important but unresolved question concerns the consequence of disrupted interhemispheric functional connectivity for a strongly lateralized cognitive function like skilled tool use. Given the neuroimaging evidence for right hemisphere activation during tool use and pantomime, as well as reports of apraxia after right-sided lesions, it is possible that pantomime impairments in the current study will correlate with disrupted connectivity between the left hemisphere tool use network and its right hemisphere homologue, or among nodes of the homologous right hemisphere network itself. Such findings would suggest a greater role for the right hemisphere in skilled tool use than previously acknowledged.

2. Materials and methods

2.1. Participants

We recruited chronic left hemisphere stroke patients from the Neuro-Cognitive Rehabilitation Research Registry at Moss Rehabilitation Research Institute (Schwartz et al., 2005). Patients whose lesions included right hemisphere areas were excluded, as were patients older than 80 years old, those who were not pre-morbidly right hand dominant, and those with any history of co-morbid or pre-morbid neurologic disorders, alcohol or drug abuse, or psychosis. Additionally, to ensure that patients understood instructions, we excluded patients with severe comprehension deficits (scores of 4 or lower on the comprehension subtest of the Western Aphasia Battery) (Kertesz, 1982). Fig. 1 displays patients' lesions on the Colin27 single-subject brain. Critically, patients were not selected based on apraxia severity, and performance on the experimental tasks spanned a range of accuracy (see Results). After excluding two patients due to the presence of a hardware imaging artifact in the functional MRI (fMRI) data, 35 patients participated (46% female; mean age = 55.8 years, SD = 11.0, range = 31–79 years). All patients were scanned at least 4.5 months after stroke, with all but one scanned 6 months or more afterwards (mean duration = 3.41 years, median duration = 1.84 years).

In addition, two groups of neurologically-intact control participants were recruited at the University of Pennsylvania. One group consisted of 13 younger participants (77% female; mean age = 22.8 years, SD = 2.1, range = 20–27 years). The second group consisted of 14 older participants (71% female; mean age = 63.3 years, SD = 6.3, range = 53–72 years). All control participants were right-handed, and we excluded any control participant with history of neurologic disorders, alcohol or drug abuse, or psychosis. While older controls were significantly older than stroke patients (Wilcoxon Rank Sum test: $P < .02$), the median ages of the combined control participants did not differ significantly from patients (control median age = 53, patient median age = 55.6; Wilcoxon Rank Sum test: $P < .09$). Functional connectivity analyses also included age as a covariate of no interest, and the age ranges of the controls and patients were substantially overlapping (important for covariate-based analyses).

All patients gave informed consent to participate in the behavioral portion of the experiment in accordance with the guidelines of the Institutional Review Board of Einstein Healthcare Network. In addition, all patient and control participants provided informed consent to participate in an MRI scanning protocol in accordance with the guidelines of the Institutional Review Board at the University of Pennsylvania. All participants were paid for their participation. In a previous study (Watson and Buxbaum, 2015), we reported behavioral and lesion data for 19 of the 35 patients in the current study.

Fig. 2. Example stimuli used in the pantomime task with patients. Examples of photographs used in the experimental tasks: A) tools used and grasped with the same hand actions ("non-conflict" tools), and B) tools used and grasped with different hand actions ("conflict" tools).

2.2. Experimental stimuli and tasks

Stimuli consisted of color photographs of tools selected from the Bank of Standardized Stimuli (BOSS) (Brodeur et al., 2010). We selected 18 "conflict" and 20 "non-conflict" tools that differed significantly on "the extent to which the hand movements that you make to use the object differ from the hand movements that you make to pick it up" but did not differ in terms of affordance strength (i.e., "the degree to which the shape of the object implies how it should be used"), name agreement, or familiarity (see Watson and Buxbaum, 2015 for further details). Examples of conflict and non-conflict tools are shown in Fig. 2.

Only stroke patients completed the behavioral portion of the experiment. On each trial, patients saw a color photograph of a tool on the screen and were instructed to "show how you would use the object". Given the possibility of right hemiparesis, patients pantomimed using their left hands. Patients completed 4 practice trials with feedback, and the experimenter advanced to the next trial if a patient said that he/she did not recognize a tool on the screen. Details on accuracy coding have been published previously (Watson and Buxbaum, 2015) and are included here in the Supplementary Materials and Methods.

2.3. MRI acquisition

MRI data were collected on a Siemens Trio 3-Tesla whole-body MRI scanner with an 8-channel head coil at the Hospital of the University of Pennsylvania using standard imaging procedures. For all participants, we collected a high-resolution, whole-brain T_1-weighted anatomical image (repetition time, TR = 1620 ms; echo time, TE = 3.87 ms; field of view, FOV = 192 × 256 mm^2; 1.0 mm^3 voxels). Spontaneous, slowly fluctuating brain activity at rest was measured during fMRI using a gradient-echo echo-planar imaging (EPI) series with whole-brain coverage (TR = 3000 ms; TE = 30 ms; FOV = 192 × 192 mm^2; 64 × 64 matrix, 48 axial slices, 3.0 mm^3 voxels). Participants were instructed to lie still and rest quietly with their eyes open. Patients were administered two separate resting-state runs in a session (run length = 100 TRs, or 5 min), while control participants received a single 5-minute run. Patients' lesions were segmented using the anatomical image and were used in voxel-based lesion-symptom mapping analyses according to previously established methods (Watson and Buxbaum, 2015; see Supplementary Materials and Methods for details).

2.4. Functional MRI preprocessing

A pictorial overview of preprocessing and analysis steps is provided in Supplementary Fig. 1. Preprocessing of the resting-state EPI scans was done within AFNI (Cox, 1996). First, large transients in the resting-state time series (due to factors such as head motion and hardware artifacts) were attenuated using 3dDespike. Time series were then corrected for slice-time acquisition (3dTshift), and all EPI volumes were co-registered with the anatomical scan (3dvolreg). Anatomical scans were segmented into gray matter, white matter, and CSF using AFNI's 3dSeg, resampling this parcellation to the EPI resolution. The white matter and CSF masks were eroded by one voxel to reduce partial volume effects with gray matter, and the white matter masks were edited to remove any subcortical structures incorrectly included as white matter (e.g., thalamus, basal ganglia). The eroded white matter and CSF time series were then applied to the volume-registered data to derive time series for nuisance regression. A voxel-specific "local" white matter regressor was formed by averaging all white matter voxel time series within a radius of 20 mm centered on each voxel (using 3dLocalStat; e.g., Jo et al., 2010; Gotts et al., 2012), and a single CSF time series was formed as an average of all time series in the eroded CSF mask (using 3dmaskave). Additionally, three aCompCor regressors (Behzadi et al., 2007) were formed as the first three principal components of the voxelwise time series data from the white matter and CSF masks, aiding in the removal of cardiac and respiratory artifacts (e.g., Stoddard et al., 2016). The volume-registered data were then spatially blurred by a 6-mm full-width at half-maximum Gaussian kernel (3dmerge), with each voxel's time series normalized by its temporal mean to yield units of percent signal change. Linear regression (3dTfitter) was used at each voxel to remove six motion parameters, one local white matter regressor, one CSF regressor, and three aCompCor regressors, with 4th-order polynomial detrending applied to both the time series data and the nuisance regressors (3dDetrend) to remove slow signal drift. The de-noised, blurred, residual time series were then transformed to Talairach space using the corresponding anatomical scan (@auto_tlrc and adwarp). An index of transient head motion (@1dDiffMag) comparable to mean Framewise Displacement (Power et al., 2012) was calculated from the motion parameters of each scan for use as a nuisance covariate in group-level analyses.

3. Experimental design: functional MRI analyses

3.1. Determining pairs of regions correlated with apraxic behavior

After preprocessing, we conducted a whole-brain, data-driven search as in Gotts & colleagues (2012; see also Berman et al., 2016) for regions of interest showing connectivity correlated with overall pantomime accuracy and/or with conflict scores. For each patient, whole-brain "connectedness" (the average Pearson correlation) was calculated for each voxel in the scan volume with all intact (i.e., non-lesioned) gray matter voxels[2] (for similar approaches, see Cole et al., 2010; Salomon et al., 2011; Hahamy et al., 2014). For each of the two runs in the patients, connectedness was correlated across patients in a voxel-wise manner with both behavioral measures (3dTcorr1D). The resulting run-specific correlation maps were then thresholded over a range of two-tailed, voxelwise p-values (from $P < .05$ to $P < .0005$) and conjoined between runs. Correction for whole-brain comparisons of the conjunction maps was then carried out using permutation tests on cluster size by randomly scrambling the runs and behavioral scores across subjects and recalculating the conjunctions (5000 iterations, e.g.,

[2] Connectedness was calculated using custom scripts rather than with AFNI's 3dTcorrMap (for improved speed and to allow calculation for non-mask values). While lesioned voxels were not part of the gray matter voxel cohort used to calculate connectedness, all voxels in the scanning volume, including lesioned voxels and those outside of the head, contained connectedness values which represented the average Pearson correlation with all non-lesioned gray matter voxels. Using different voxel cohorts for each participant to calculate connectedness could have potentially impacted the seed detection process, although control analyses matching voxel cohorts across all participants (all right hemisphere gray matter voxels) yielded the same selection of seeds, suggesting that the current approach did not result in undue bias.

Maris and Oostenveld, 2007; Eklund et al., 2016; implemented in MATLAB and tcsh with AFNI commands). Detected clusters can then be used as seeds in more traditional seed-to-whole-brain correlation tests to determine which other voxels are most responsible for driving the results in whole-brain connectedness, with simultaneous correction for voxel-wise tests and the number of seeds tested by permutation (see Gotts et al., 2012; Meoded et al., 2015; Song et al., 2015; Berman et al., 2016; Stoddard et al., 2016 for further examples/discussion).

To examine whether region-by-region pairs showing correlations with apraxic behaviors were also impaired relative to age- and motion-matched controls, we also conducted *t*-tests between patients and controls in the seed-based and region-to-region tests. For these tests, the two patient runs were concatenated into a single longer run. The group comparisons were similarly thresholded at a variety of *p*-values and corrected by permutation testing (5000 iterations). Behavioral correlations in the patients were only considered further if the connections were also significantly different between patients and controls ($P < .05$, corrected).

After determining the number of seeds in the connectedness tests, along with additional regions identified during seed testing in two sets of tests (overall accuracy and conflict scores), a full region-by-region matrix was constructed. Each cell of the matrix was tested for behavioral correlations within the patient group using both behavioral measures, as well as for group differences between patients and controls, all using Age and Motion as nuisance covariates (partial correlations for correlations with behavior; *t*-tests with covariates, 3dttest++, for group comparisons). For both behavioral measures, correlations were corrected for multiple comparisons in each run separately using False Discovery Rate (FDR, e.g., Genovese et al., 2002). A common FDR threshold was determined across both behavioral measures and both runs for these purposes. Only region-by-region pairs that replicated across runs (FDR-corrected in each run to $q < 0.05$; critical *p*-value of $P < .0021$) and that also differed between patients and controls at $P < .05$ are reported.

Results in this region-by-region matrix were also further checked for other potential confounding factors. In addition to Age and Motion, sensitivity of the results was checked to lesion size (log lesion volume[3]), to the grand average correlation level over all voxelwise combinations, or GCOR (Saad et al., 2013, @compute_gcor), and to the average voxelwise signal amplitude (standard deviation; 3dTstat) (see Gotts et al., 2018 for discussion). For these post-hoc control analyses, given that additional degrees of freedom were being lost due to the covariates, we only required replication at a level of $P < .05$ across runs (although still requiring group differences of $P < .05$).

3.2. Determining relative contributions of lesions and whole-brain connectedness to behavioral results

VLSM analyses have previously been used to examine how the presence versus absence of lesions in a given voxel is associated with behavioral impairment (e.g., Watson and Buxbaum, 2015). In the current study, we examined the relative contributions of VLSM and functional connectivity analyses in explaining behavior by combining VLSM (*t*-tests between lesioned and non-lesioned groups on a behavioral measure) and continuous correlations with behavior (Pearson *r*-tests) into a single statistical model using R^2. Complete details on the R^2 modeling approach is provided in the Supplementary Materials and Methods.

[3] Given the right-skewed distribution of lesion volume in our sample, we used the log transform of lesion volume in order to improve normality. However, all results are comparable when using raw lesion volume, instead.

4. Results

4.1. Functional connectivity measures predict apraxic behavior

First, we examined whole-brain correlations between each measure of apraxia and "connectedness" values. Results for overall accuracy on the pantomime task are shown in Fig. 3 (mean accuracy = 84%, SD = 11, range = 55%–99%). Three seeds were significant in whole-brain connectedness in both runs and survived permutation testing at a voxelwise threshold of $P < .05$ (corrected by cluster size to $P < .05$): the left superior parietal cortex and postcentral gyrus (Seed 1 in Fig. 3), the left thalamus (Seed 2), and the left pMTG (Seed 3). The corresponding seed-based results are also shown in Fig. 3, with correlations with overall accuracy presented in the first row for each seed (conjoined across runs at the *p*-value given by the corresponding color bar to the left, and corrected to $P < .05$ by permutation for three whole-brain, voxelwise tests), while the differences between patients and controls are presented in the second row for each seed. Correlations with overall accuracy were uniformly positive, indicating that greater functional connectivity was associated with better accuracy in the pantomime task. Similarly, functional connectivity between these same regions was often significantly weaker in patients than in controls; no regions showed significantly greater functional connectivity in patients.

Analogous results for correlations with conflict scores are shown in Fig. 4 (mean conflict score = 0, SD = 0.96, range = −1.94–1.56). Two seeds were significant in whole-brain connectedness in both runs and survived permutation testing at a voxelwise threshold of $P < .05$ (corrected by cluster size to $P < .05$): left SMG, ventral pre- and postcentral gyri, and ventral premotor cortex (Seed 1, Fig. 4), and left dorsal pre- and postcentral gyri (Seed 2, Fig. 4), just anterior to the superior parietal seed correlated with overall accuracy (Seed 1, Fig. 3). As with overall accuracy, the seed-based results highlighted regions with a similar spatial distribution in both the conflict score correlations (all of which were positive) and those that differed between patients and controls (all of which showed significantly weaker functional connectivity).

To arrive at a final set of regions of interest for further examination, we used a voxelwise threshold ($P < .005$) on the seed-based tests that was stringent enough to break up the largest clusters (corrected to $P < .05$), and we further required that functional connectivity differ between patients and controls (corrected to $P < .05$). Pooling regions of interest across the overall accuracy and conflict score analyses, this resulted in 32 regions. Fig. 5 shows these regions, coded by color to indicate which effect was associated with each (yellow: overall accuracy only; blue: conflict scores only; red: involved in both effects) (see Supplementary Fig. 2 for a rendering of these regions on the cortical surface). The region-by-region matrix in the right panel of Fig. 5 organizes the regions by hemisphere (row/column order of regions shown in Table 1) and shows which region-by-region combinations replicate across runs ($P < .0021$ to be FDR-corrected in each run separately to $q < .05$). These combinations further had to differ significantly between patients and controls ($P < .05$), covarying nuisance measures of transient head motion and age for all tests (partial correlations for behavioral results; two-sample *t*-tests with covariates for the group comparisons). Correlations with overall accuracy appeared to have prominent involvement of right hemisphere in addition to left hemisphere regions, whereas correlations with conflict score involved left hemisphere regions more selectively.

To visualize more easily the region-by-region relationships shown in the matrix of Fig. 5, these relationships were then rendered in the brain using hub-and-spoke diagrams in Fig. 6. All region-by-region relationships are depicted. Panels were created by selecting regions with the largest number of connections in the matrix; these tended to be the main seeds. The size of each circle in Fig. 6 is proportional to a region's volume in terms of number of voxels (see key in bottom right of Fig. 6). Lines connect regions for which functional connectivity is significantly

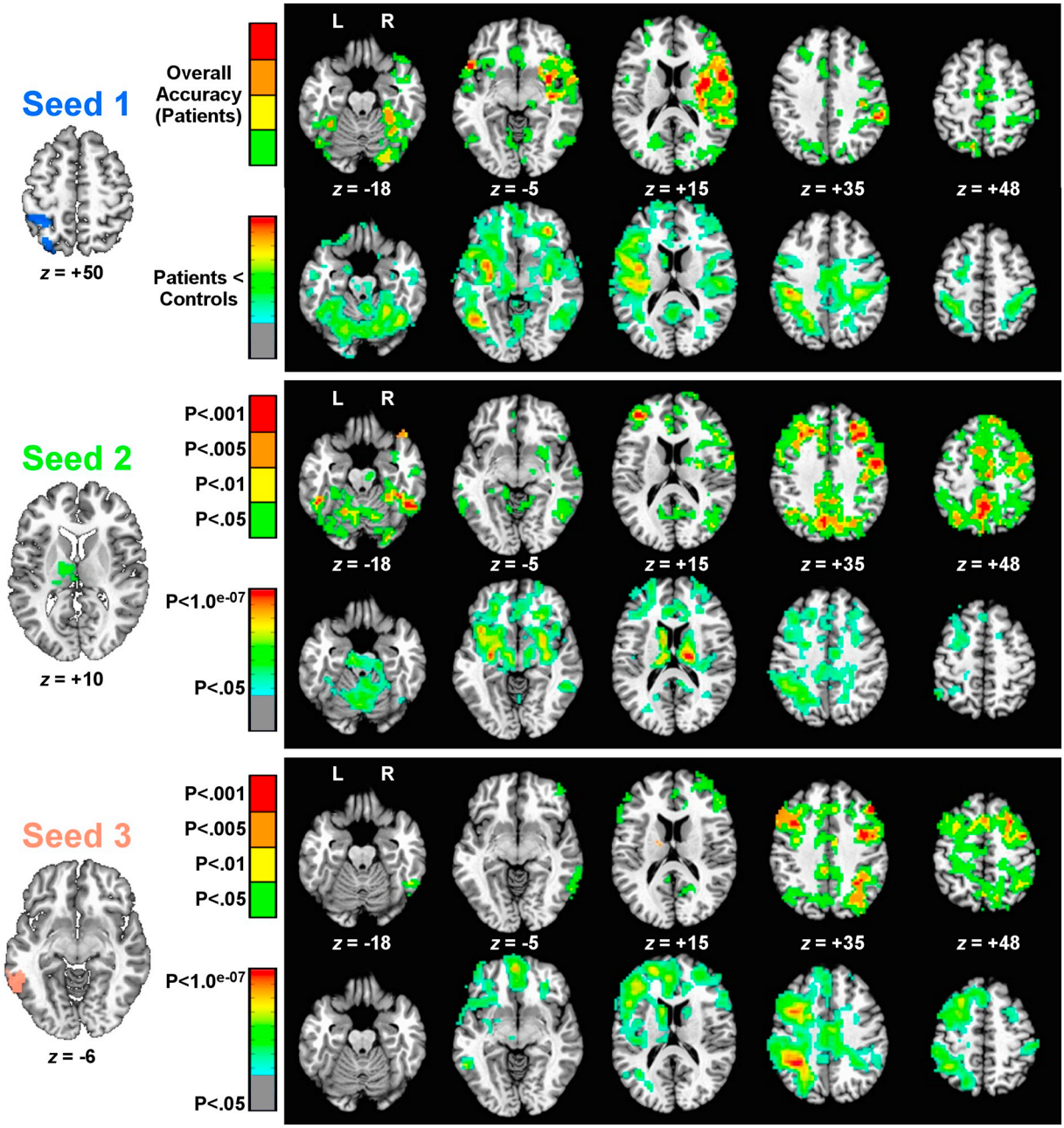

Fig. 3. Seed detection and testing related to overall accuracy in the pantomime task. The three seeds found in correlations between overall accuracy and whole-brain connectedness are shown to the left. For each seed, two rows of corresponding seed-to-whole-brain results are shown to the right. The top row for each seed shows permutation-corrected results (cluster size) of seed-to-voxel functional connectivity that is positively correlated with overall accuracy at differing levels of significance (levels of $P < .05$ down to $P < .001$). The colors indicate the lowest p-value in this range that was found to be significant (from green, $P < .05$, ranging down to red, $P < .001$). The second row for each seed shows permutation-corrected group comparisons of patients versus controls ($P < .05$, 2-tailed) for seed-to-voxel functional connectivity. In all cases, these group comparisons followed the pattern of patients < controls (weaker functional connectivity in patients), with voxelwise significance level shown using color (p-values ranging from green, $P < .05$, down to red, $P < .1.0 \times 10^{-07}$). As the group comparisons were also false-discovery rate (FDR) corrected at a voxelwise threshold of $P < .05$ ($q < .05$), the significance level for these plots is shown on a continuous scale rather than at discrete intervals. For inclusion in later analyses, all behavioral correlations had to survive at least a $P < .005$ threshold in both runs and additionally show a significant difference between patients and controls ($P < .05$).

correlated with either overall accuracy (yellow circles) or conflict scores (blue circles). Regions that are involved in both effects are rendered in red (see Supplementary Fig. 3 for axial, sagittal, and coronal views with all connections plotted simultaneously). For the axial brain plots on the left, the top and middle rows depict results related to overall accuracy. In brief, the top left axial plot shows that higher overall accuracy is correlated with greater functional connectivity between the left pMTG seed and the dorsolateral prefrontal cortex (DLPFC) bilaterally, the anterior cingulate cortex, and the right dorsal premotor cortex and intraparietal sulcus. The top right axial plot shows that overall accuracy is also correlated with functional connectivity between the left thalamus seed and bilateral DLPFC and medial prefrontal cortex (anterior cingulate cortex and cingulate gyrus), as well as with the right medial portion of the fusiform gyrus, extending into the cerebellum. The left middle axial plot depicts the correlation between overall accuracy and functional connectivity between the left superior

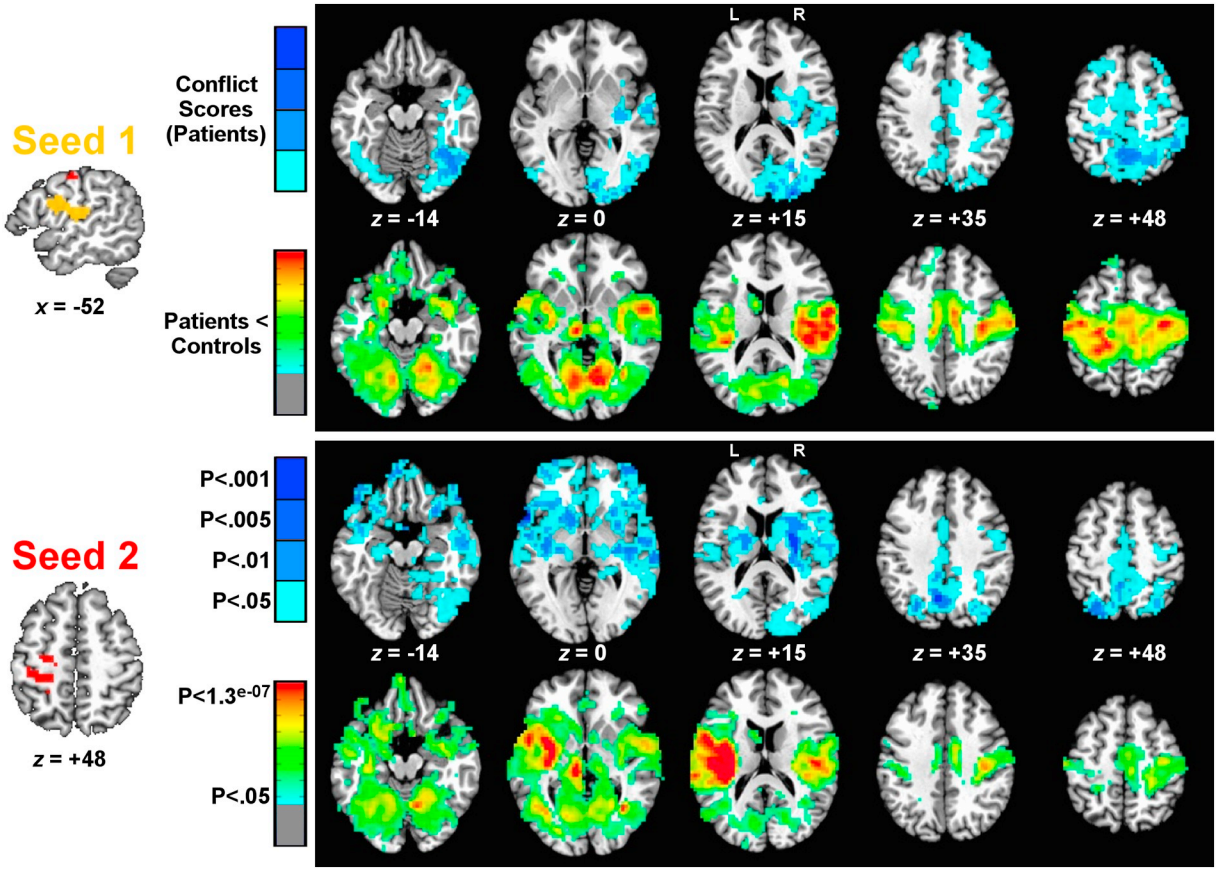

Fig. 4. Seed detection and testing related to object conflict scores. The two seeds found in correlations between overall accuracy and whole-brain connectedness are shown to the left. For each seed, two rows of corresponding seed-to-whole-brain results are shown to the right. The top row for each seed shows permutation-corrected results (cluster size) of seed-to-voxel functional connectivity that is positively correlated with conflict score (greater functional connectivity - > better performance on objects with different use and grasp actions) at differing levels of significance (levels of $P < .05$ down to $P < .001$). The colors indicate the lowest p-value in this range that was found to be significant (from light blue, $P < .05$, ranging down to dark blue, $P < .001$). The second row for each seed shows permutation-corrected group comparisons of patients versus controls ($P < .05$, 2-tailed) for seed-to-voxel functional connectivity. In all cases, these group comparisons followed the pattern of patients < controls (weaker functional connectivity in patients), with voxelwise significance level shown using color (p-values ranging from green, $P < .05$, down to red, $P < .1.3 \times 10^{-07}$). As the group comparisons were also false-discovery rate (FDR) corrected at a voxelwise threshold of $P < .05$ ($q < .05$), the significance level for these plots is shown on a continuous scale rather than at discrete intervals. For inclusion in later analyses, all behavioral correlations had to survive at least a $P < .005$ threshold in both runs and additionally show a significant difference between patients and controls ($P < .05$). (For interpretation of the references to color in this figure legend, the reader is referred to the web version of this article.)

parietal cortex seed and the left medial fusiform gyrus and right insula/putamen, anterior insula, postcentral gyrus, ventral premotor cortex, superior temporal gyrus, lateral occipitotemporal cortex, and SMG. Finally, the right middle axial plot shows that overall accuracy is also correlated with functional connectivity between the left pre- and postcentral gyri and the right mid-insula and putamen.

The bottom row of Fig. 6 depicts the results for conflict scores, with the left panel showing that better performance on conflict relative to non-conflict tools on the pantomime task is significantly correlated with functional connectivity between the left pre- and postcentral gyri seed and left ventral IFG, insula, putamen/caudate, ventromedial prefrontal cortex, and bilateral superior temporal gyrus. The bottom right panel shows that conflict scores are also correlated with functional connectivity between the left peri-Sylvian seed covering SMG/ventral pre- and postcentral gyri/ventral premotor cortex and right lateral occipitotemporal cortex.

The right panels of Fig. 6 use histograms to show the distribution of regions at the voxel level by X-, Y-, and Z-coordinates in Talairach space. While voxels from regions associated exclusively with overall accuracy (yellow histograms in the left column) are well-distributed along every dimension, voxels from regions associated exclusively with the conflict score (blue histograms) are more left-lateralized (i.e., negative X-coordinates) and peri-Sylvian (i.e., small positive Y- and Z-coordinates).

4.2. Relative contributions of lesion location and functional connectivity to behavioral correlations

In the analyses above, whole-brain connectedness values were calculated across all brain voxels, including those that were lesioned for a given patient. While it is not obvious how selective functional connectivity patterns could be repeatedly correlated with behavior from locations with little or no residual brain tissue, we nevertheless conducted several follow-up analyses to examine the contribution of lesioned voxels to the results. First, we covaried lesion size (log lesion volume) as a nuisance variable from the correlations with overall accuracy and conflict scores (see Supplementary Fig. 4). This had little or no influence on the pattern of results in Fig. 5, with all reported behavioral correlations continuing to replicate across runs at a level of $P < .05$. Similarly, covarying other artifact measures such as age, motion, the global level of correlation (GCOR, Saad et al., 2013), and a measure of average temporal signal-to-noise ratio had little or no influence on the results (see Supplementary Results and Supplementary Fig. 4).

As a second and more direct test, we recalculated each patient's average regional time series from the 32 regions of interest after

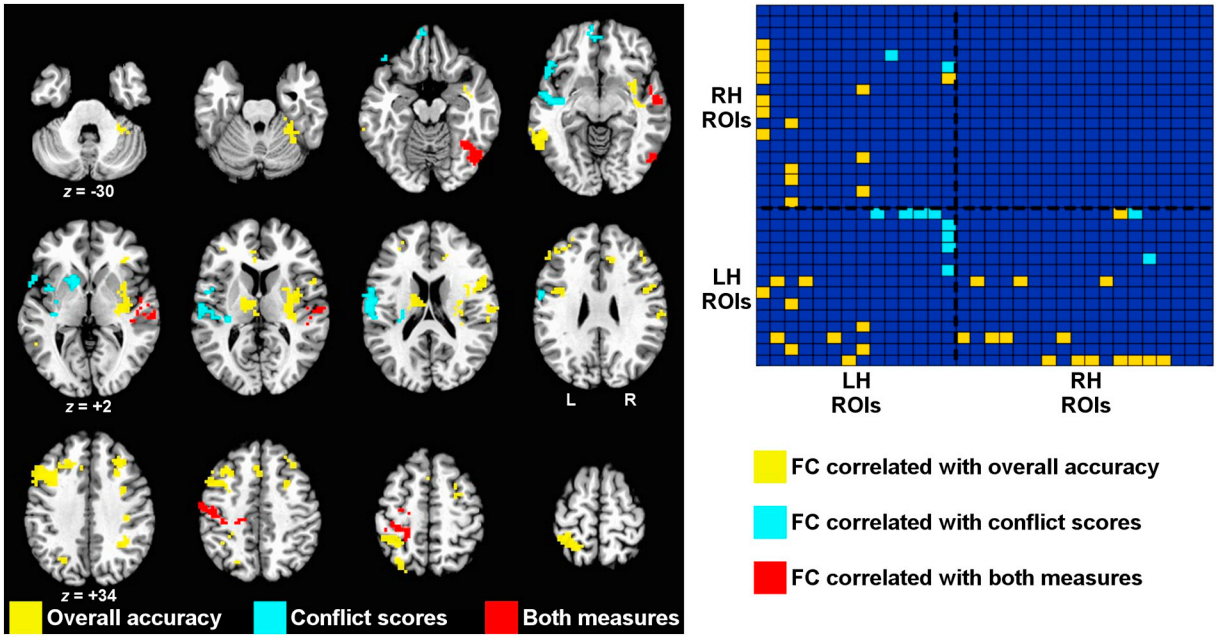

Fig. 5. Consolidated set of regions of interest across correlations with overall accuracy and conflict score. (Left panel) Regions involved only in overall accuracy effects are shown in yellow, regions involved in only conflict score effects are shown in light blue, and regions involved in both types of effects are shown in red. (Right panel) Matrix of region-by-region interrelationships that exhibit correlations with overall accuracy and conflict score. Regions are ordered left-to-right and bottom-to-top first by hemisphere (LH = left hemisphere, RH = right hemisphere), and then within hemisphere, by which type of effect the regions were associated with in the volume-based analyses. Row/column order of the regional labels is given in Table 1. A colored square in the matrix indicates that effects replicated across runs at an FDR-corrected threshold ($P < .0021$, 2-tailed, $q < .05$) and also showed a significant effect of group ($P < .05$, 2-tailed). Note that the absence of red squares in the right panel but presence of red regions in the left panel indicates that while there were no *pairs* of regions whose functional connectivity correlated with both behavioral measures, some regions were involved in both effects as part of different pairs. (For interpretation of the references to color in this figure legend, the reader is referred to the web version of this article.)

excluding all lesioned voxels from the averages. Regional data were included for a given patient provided that the lesioned voxels did not make up > 75% of the original region, with behavioral correlations for a given region-to-region pair calculated over all patients with available data. All but one region had at least 30 patients with included data; the left inferior frontal junction had only 20/35 patients with included data, and the relationship with this region and left pMTG was therefore excluded from this analysis. All of the remaining reported behavioral correlations in the region-by-region matrix of Fig. 5 continued to replicate across runs at a level of $P < .05$ or less (see Supplementary Table 1). It is therefore unlikely that the reported results are a simple result of the lesioned voxels themselves—which certainly cannot be the case for right hemisphere regions, all of which were free of lesions in all patients. A more likely explanation is that the functional connectivity results in the lesioned left hemisphere reflect alterations in the spared physiological interactions of tissue adjacent to (or functionally connected with) the lesioned tissue.

However, given that previous VLSM studies have demonstrated correlations of lesion location with overall accuracy and with conflict scores in similar regions to those reported above (Watson and Buxbaum, 2015), we wanted to quantify the separable contributions of lesion and functional connectivity measures to correlations with these two behavioral measures. Therefore, we combined the lesion and whole-brain connectedness information in one model using an R^2 approach, calculating the variance explained by the VLSM model and the unique variance attributable to connectedness after partialling out the VLSM model. Results of this analysis are shown in Fig. 7 within the mask of lesion locations analyzed by VLSM (i.e., voxels in which at least five patients had a lesion), with results for overall accuracy shown in the top panels and for conflict score in the bottom panels. The left column depicts the amount of variance in the behavioral measures (in terms of R^2) explained by the VLSM model. In contrast, the middle column shows the total variance explained by the combined VLSM + connectedness model, with clear increases in the variance explained throughout much of the analysis mask. The right column shows the unique contributions of connectedness to R^2 that remain significant after partialling out the VLSM model. For overall accuracy (top right panel of Fig. 7), connectedness contributed unique variance in the left superior parietal cortex ($P < .05$, corrected by permutation), largely identical to Seed 1 in Fig. 3. Similarly, connectedness contributed unique variance in the conflict score (bottom right panel of Fig. 7) in left pre- and postcentral gyri and left SMG/ventral pre- and postcentral gyri/ventral premotor cortex, comparable to Seeds 1 and 2 in Fig. 4.

Taken together, these results establish that the functional connectivity results reported in the current paper are unlikely to be due to the inclusion of lesioned tissue in the analyses. Rather, the functional connectivity results appear to provide a unique contribution to the explanation of apraxic behavior beyond the information provided by the lesions. Models that include both anatomical and physiological information should therefore provide a better account of patient behavior than either type of information in isolation.

5. Discussion

This study used a data-driven approach (Gotts et al., 2012) to explore correlations between apraxia following left hemisphere stroke and spontaneous, resting brain activity in fMRI using two indices: overall accuracy on a tool use pantomime task, and a measure that reflects the ability to select a *use* action despite competition from a different *grasp-to-move* action associated with the same tool (i.e., conflict scores). Both measures—and particularly, overall accuracy—correlated with the strength of functional connectivity between left hemisphere regions associated with tool use and action production (including pMTG, SMG, posterior medial fusiform gyrus, lateral occipitotemporal cortex, superior parietal lobe, pre- and postcentral gyri, and ventral premotor cortex), on the one hand, and regions located in the right hemisphere,

Table 1
Order and description of 32 regions-of-interest shown in region-by-region matrix in Fig. 5.

Order	Side	Centroid			Description	Number of voxels
		x	*y*	*z*		
1	L	−28	−52	53	Superior parietal lobe, postcentral gyrus	220
2	L	−36	23	34	Dorsolateral prefrontal cortex	232
3	L	−56	−48	−5	Posterior middle temporal gyrus	71
4	L	−5	36	9	Anterior cingulate cortex	12
5	L	−8	−37	33	Posterior cingulate, supplementary motor area	12
6	L	−37	−1	27	Inferior frontal junction	10
7	L	−32	−45	−17	Fusiform cortex	9
8	L	−11	−13	13	Thalamus	69
9	L	−48	16	−3	Superior temporal gyrus, inferior frontal gyrus	58
10	L	−50	−13	16	Pre- & postcentral gyri, supramarginal gyrus, ventral premotor cortex	152
11	L	−40	−12	−4	Superior temporal gyrus, insula	61
12	L	−15	9	2	Putamen, caudate	27
13	L	−6	51	−9	Ventromedial prefrontal cortex	22
14	L	−31	−25	45	Pre- & postcentral gyri	99
15	L	−2	20	42	Anterior cingulate cortex	27
16	R	29	27	36	Dorsolateral prefrontal cortex	59
17	R	28	5	44	Dorsal premotor cortex	34
18	R	33	−47	34	Intraparietal sulcus	32
19	R	12	32	23	Anterior cingulate cortex, cingulate gyrus	14
20	R	15	−59	−12	Medial occipital cortex, cerebellum	12
21	R	35	30	3	Anterior insula	11
22	R	43	33	26	Dorsolateral prefrontal cortex	9
23	R	37	−24	35	Postcentral gyrus	8
24	R	49	5	20	Ventral premotor cortex	52
25	R	31	−40	−24	Fusiform cortex, cerebellum	80
26	R	33	−7	5	Insula, putamen	252
27	R	53	−15	1	Superior temporal gyrus	101
28	R	43	−60	−11	Lateral occipitotemporal cortex, fusiform gyrus	68
29	R	57	−21	21	Supramarginal gyrus, postcentral gyrus	39
30	R	8	−82	10	Occipital cortex (pericalcarine)	19
31	R	32	−84	7	Middle occipital cortex	19
32	R	9	−52	50	Precuneus	10

Coordinates reported in Talairach standardized space. Voxel size = 3 mm^3. Order of regions in table corresponds to the left-right and bottom-top order of regions in region-by-region matrix in Fig. 5.

on the other. Often, these interhemispheric functional connections implicated right hemisphere homologues of left hemisphere regions associated with tool use and action. The status of interhemispheric functional connectivity continued to be associated with apraxic deficits in a secondary analysis designed to eliminate the influence of lesioned tissue on the results, and the reported effects also persisted after explicitly controlling for other residual global artifacts. Yet, we also observed differences in the patterns of functional connectivity correlated with each measure of apraxia. Overall accuracy on the pantomime task was associated with functional connectivity among a broadly-distributed set of bilateral regions, while the conflict score was associated with functional connectivity among a relatively left-lateralized and peri-Sylvian set of areas. Finally, performance on both measures was best predicted by a model incorporating information about both lesion location and functional connectedness, with functional connectivity explaining unique variance in behavior even among voxels in the lesioned left hemisphere. These findings extend those published previously in a number of respects.

Current neuropsychological (e.g., Haaland et al., 2000; Hanna-Pladdy et al., 2001) and neuroimaging (see Lewis, 2006; Ishibashi et al., 2016 for reviews) research is in agreement that praxis relies on a left-lateralized set of brain regions. Even when demonstrating tool use with the non-paretic left hand (as in the current study), left hemisphere stroke patients continue to display apraxia, as do split-brain patients only when gesturing with the left hand (Lausberg et al., 2003), casting doubt on the ability of the right hemisphere alone to support skilled action. Yet, the existence of patients with apraxia after right hemisphere lesions (e.g., Roy et al., 2000) and the occurrence of bilateral activation in neuroimaging studies of neurologically-intact participants (e.g., Hermsdörfer et al., 2007) continues to evoke debate on the role of the right hemisphere in skilled action. In the current study, the status of interhemispheric functional connectivity predicted apraxic behavior, indicating a larger role for the right hemisphere in tool use than typically acknowledged. Particularly important was the correlation of overall pantomime accuracy with functional connectivity between two left hemisphere regions (left pMTG and thalamus) and a largely common, bilateral set of regions in DLPFC and medial prefrontal cortex. Accuracy also correlated with connectivity between left superior parietal cortex and pre- and postcentral gyri, on the one hand, and an almost entirely right-lateralized set of regions on the other, including right insula/putamen, postcentral gyrus, ventral premotor cortex, lateral occipitotemporal cortex, SMG, and superior temporal gyrus.

Our results echo numerous recent studies in other cognitive domains that have identified the importance of interhemispheric functional connectivity in predicting deficits following stroke (for a review, see Baldassarre et al., 2016). For example, disrupted interhemispheric functional connectivity immediately following left or right hemisphere stroke correlates with measures of lower-level motor function and attention (Carter et al., 2010; Hayward et al., 2017). In fact, a recent fMRI study of resting functional connectivity in 132 sub-acute stroke patients identified decreased interhemispheric functional connectivity as common to impaired performance across all domains tested (attention, visual/verbal memory, motor, visual, and language) (Siegel et al., 2016). Similarly, a recent task-based fMRI study of left hemisphere stroke patients found that apraxia correlated with the magnitude of activation evoked by the observation of tool action videos in left hemisphere parts of the tool use network and, when lesion volume was added as a covariate, other areas that included right IFG and dorsal premotor cortex (Martin et al., 2016). Together with the present results, this suggests that processing within the right hemisphere and communication between hemispheres is necessary for successful tool-related action.

In the current study, interhemispheric functional connectivity correlated positively with performance on tests of apraxia, despite the known left-lateralization of the typical praxis network. Language—another strongly left-lateralized cognitive function—is similarly impaired following the disruption of communication between hemispheres (Siegel et al., 2016). However, unlike other cognitive domains examined in this study, language impairments also relied on the strength of intrahemispheric functional connectivity within the left hemisphere. Also dissimilar to other domains, lesion location and functional connectivity were both useful predictors of language impairments. Siegel et al. (2016) suggest that language impairments can arise both from the disruption of language-specific processes and from the disruption of “bilaterally distributed support processes” (p. 6). The similarity of the current study's results may not be a coincidence: a growing number of studies highlight parallels—and overlaps—between networks for language and praxis. Approximately two-thirds of patients with aphasia are also apraxic (Weiss et al., 2016), and the neurobiological organization of spoken language is largely shared with sign language (Hickok et al., 1998) and symbolic gesture processing (Xu et al., 2009). Accordingly, a recent two route model of praxis (Buxbaum, 2017; Buxbaum and Randerath, 2018) explicitly invokes parallels with similar two-route models in the language domain (e.g., Hickok and Poeppel, 2004, 2007; Saur et al., 2008). Thus, the present results indicate that while the status of interhemispheric functional

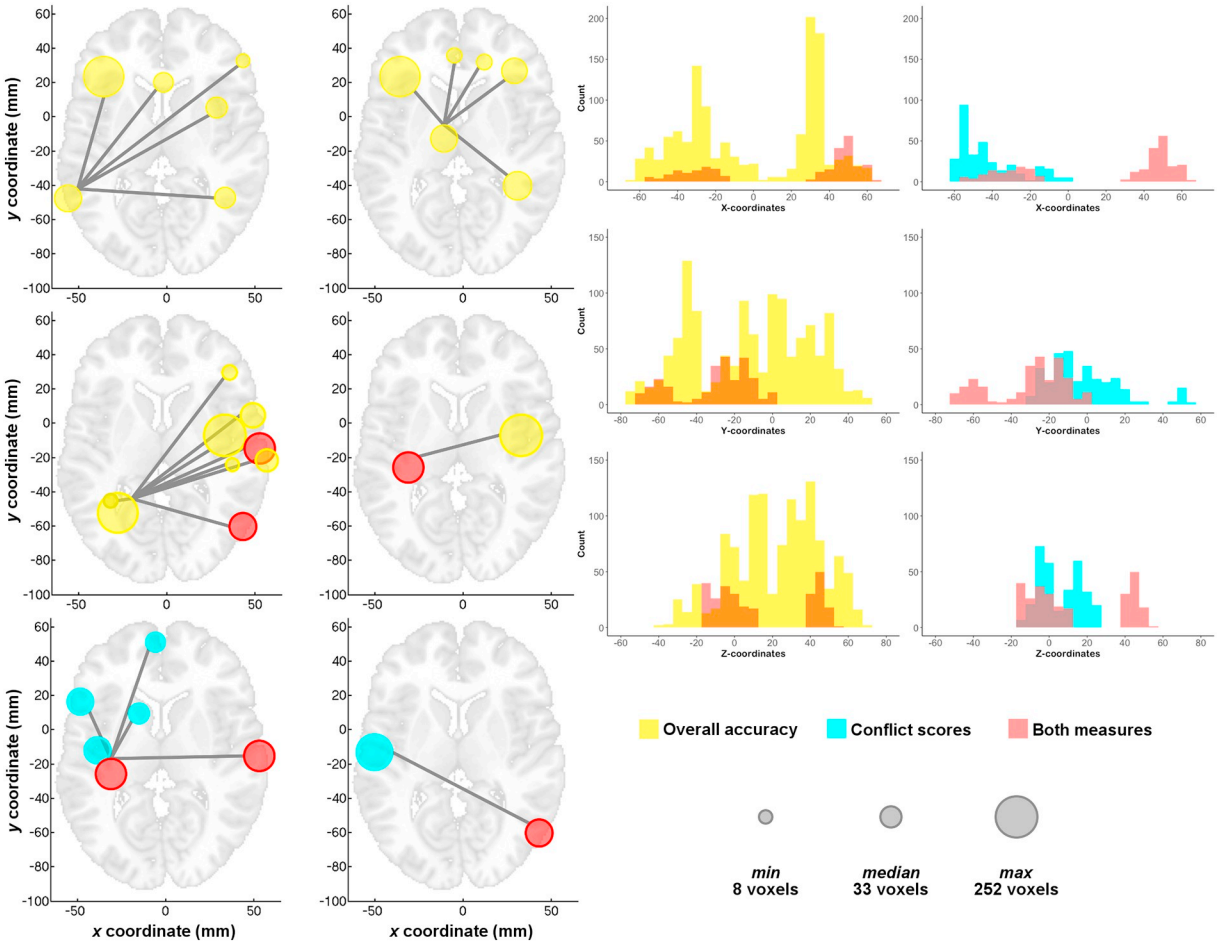

Fig. 6. Correlations with overall pantomime accuracy are strongly bilateral, whereas correlations with conflict scores are more left-lateralized. (Left panels) The matrix relationships shown in Fig. 5 are plotted by panel for different regions involved in the greatest number of effects to aid visualization in the brain volume. Views are axial, with left = left. Corresponding depiction for axial, sagittal, and coronal views is provided in Supplementary Fig. 3. Color scheme is as in Fig. 5. Size of the colored circles in terms of the number of voxels follows the key shown to the bottom right of the figure (gray circles). (Right panels) Histograms of voxel counts by X-, Y-, and *Z*-coordinates in Talairach-Tournoux space show differential distributions of the overall accuracy and conflict score effects by hemisphere (X-coordinate). Voxels involved in overall accuracy effects have a similar distribution in the two hemispheres, whereas voxels involved only in conflict score effects are more left-lateralized.

connectivity is likely to be predictive of impairments across domains, language and praxis also uniquely rely on intact functional connectivity within the left hemisphere.

Critically, patients in the current study were in the chronic stage of recovery. Moreover, all voxels and regions whose average functional connectivity was significantly different in stroke versus control participants reflected functional connectivity that was *weaker* in patients than controls. Therefore, our results are not likely to reflect new functional connections formed after stroke or the organization of an atypical network. Further, in other studies, the degree of interhemispheric connectivity present even within the first weeks after stroke—unlikely to reflect reorganization—similarly correlates with behavioral deficits (He et al., 2007; Carter et al., 2010; Baldassarre et al., 2014). Although it is possible that changes in interhemispheric functional connectivity following stroke support recovery from apraxia, in the current study, MRI scans and behavioral data were not collected at time intervals to assess this question. However, using the available data, we performed an additional analysis to determine whether functional connectivity between any of our regions of interest correlated with the time between a patient's stroke and MRI scan, and none of the pairs of regions that emerged (even at a lenient threshold) overlapped with those whose functional connectivity correlated with measures of apraxia (see Supplementary Results and Supplementary Fig. 5). This pattern of results suggests that the right hemisphere involvement observed in the current study does not reflect functional connections formed during recovery. Instead, patients whose left hemisphere lesions are less disruptive of interhemispheric functional connectivity may be less apraxic. Alternatively, pre-morbid individual differences may mean that patients with stronger interhemispheric functional connectivity fare better following left hemisphere lesions.

Among the functional connections that correlated with overall degree of apraxia, we observed a number of patterns. The first pattern reflected connectivity between regions critical for cognitive control and regions involved in gesture representation and production. For example, functional connectivity between left pMTG, on the one hand, and bilateral DLPFC and medial prefrontal cortex, on the other, was associated with better pantomime performance. DLPFC and anterior cingulate cortex are both regions consistently implicated as being critical for cognitive control (e.g., MacDonald et al., 2000; Curtis and D'Esposito, 2003; Badre and Wagner, 2004; Cole and Schneider, 2007), flexible guidance of thoughts and behavior according to current goals, and demanding cognitive and semantic tasks (Duncan, 2010; Fedorenko et al., 2013; Noonan et al., 2013). Left pMTG is a critical 'hub' within the tool use network (Lewis, 2006; Martin et al., 2014; van Elk et al., 2014) and may represent knowledge of actions derived from visual experience (Kalénine et al., 2010; Watson et al., 2013; Orban and Caruana, 2014), including the typical posture and movement of the hand (Buxbaum, 2001; Buxbaum et al., 2014). Lesions here are

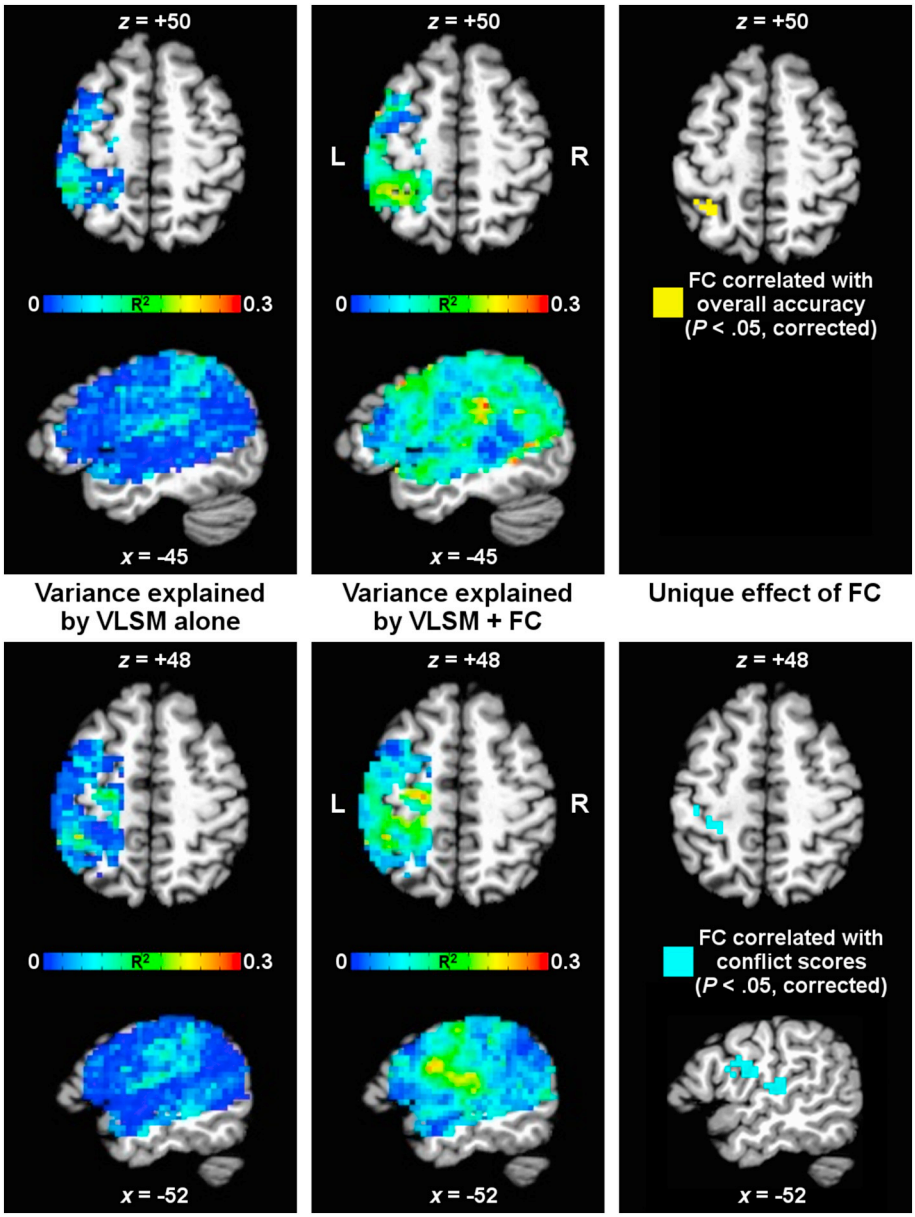

Fig. 7. Relative contributions of lesions versus functional connectivity measures to behavioral correlations. Contributions of the voxel-based lesion-symptom mapping (VLSM) model relative to whole-brain functional connectedness (FC) are shown in terms of R^2 for overall accuracy (top panels) and conflict score (bottom panels). The left-most panels show the R^2 of the behavioral measures explained by the VLSM model alone (with color indicating R^2 value). The middle panels show the total R^2 explained by both VLSM and FC combined. The right-most panels show the unique effect of FC, having removed shared variance with the VLSM model and corrected for all voxelwise comparisons in the mask by permutation testing.

associated with apraxia and gesture recognition deficits (Buxbaum et al., 2014; Tarhan et al., 2015; Watson and Buxbaum, 2015), and patterns of activity in pMTG discriminate between the preparation of different tool actions in neurologically-intact participants (Gallivan et al., 2013). Therefore, intact functional connectivity of bilateral cognitive control regions with left pMTG may be critical for enabling top-down modulation of task-relevant action processing (Botvinick et al., 2001; Miller and Cohen, 2001). Similarly, functional connectivity between the left thalamus and bilateral DLPFC/medial prefrontal cortex also correlated with overall degree of apraxia. Although apraxia following thalamic lesions has been reported (De Renzi et al., 1986; Nadeau et al., 1994), its occurrence is rare. Recent research suggests that the thalamus plays a role in integrating information between cortical regions (Hwang et al., 2017). In particular, thalamic nuclei that receive basal ganglia input may mediate information flow from prefrontal cortex to areas responsible for movement execution (Haber and Calzavara, 2009).

A second general pattern in the overall accuracy data reflected connectivity between left superior parietal and sensorimotor cortices, and right insula/putamen, ventral premotor cortex, and lateral occipitotemporal cortex—i.e., a right-lateralized homologue of the tool use network.[4] Activation is observed within the right insula during pantomimed tool use (Króliczak et al., 2007) and during body self-awareness tasks (Farrer et al., 2003), and patients with right insular lesions exhibit anosognosia for left-sided hemiplegia or hemiparesis (Karnath et al., 2005; Baier and Karnath, 2008). Thus, the right insula has been hypothesized to be critical for self-awareness of action (Karnath et al., 2005) and for working in concert with left inferior parietal cortex to create a visuospatial description of one's own body (Chaminade et al., 2005)—functions that are critical for successful tool use.

Examination of correlations between functional connectivity and the conflict score, a measure that specifically reflects the ability to

[4] It might be argued that communication with the right hemisphere was artificially important in the present study because patients pantomimed with the (unimpaired) left hand (albeit in a behavioral session separate from the fMRI scans). However, the right hemisphere is involved even when right-handed participants plan or execute tool-related actions with the right hand (Bohlhalter et al., 2009; Króliczak et al., 2016).

select use actions despite competing grasp actions associated with the same tool (Jax and Buxbaum, 2010, 2013) revealed a pattern of results that differed in two ways. First, disproportionate difficulty with conflict tools was associated with functional connectivity among a more localized peri-Sylvian set of regions relative to overall pantomime accuracy. This result replicates and extends those we previously reported based on lesion loci alone (Watson and Buxbaum, 2015), in which lesions to left SMG, IFG, and anterior insula were critical predictors of impaired tool action selection. Here, we similarly find that deficient functional connectivity between left sensorimotor areas, including peri-Sylvian SMG, ventral pre- and postcentral gyri, and ventral premotor cortex, and other left hemisphere regions, including peri-Sylvian superior temporal gyrus/IFG, correlates with the same measure. Thus, both VLSM and functional connectivity analyses implicate areas along the ventral subdivision of the traditional dorsal processing stream for action (Goodale and Milner, 1992; Milner and Goodale, 2008). This "ventro-dorsal" stream in the left hemisphere is specialized for processing skilled actions associated with familiar objects (*use* actions), while the bilateral "dorso-dorsal" stream is specialized for processing actions based on the structure of currently-viewed objects (*grasp* actions) (Binkofski and Buxbaum, 2013; Sakreida et al., 2016; Rizzolatti and Matelli, 2003). The present study indicates that functional connectivity within the left ventro-dorsal stream is particularly critical when the correct use response cannot be derived solely from tool size and shape, as is the case with "conflict" objects.

Second, disproportionate difficulty with conflict tools also correlated with functional connectivity among a more strongly left-lateralized set of regions than overall accuracy on the pantomime task. While tool use pantomime can fail due to impairments to diverse cognitive functions reliant on a broad set of brain regions—from the retrieval of stored tool use knowledge to the execution of motor commands—disproportionate difficulty with tools with competing use and grasp actions isolates a weakness in use representations—and perhaps, the ability of use representations to compete against grasp actions. Our results suggest that this competition is primarily resolved within the left hemisphere ventro-dorsal stream, perhaps because these areas represent competing candidate actions during the course of action specification and production (Watson and Buxbaum, 2015). Similarly, ventro-dorsal regions appear to integrate information from the ventral visual stream regarding object identity and information from the dorsal visual stream regarding the position of the body in space (Buxbaum et al., 2007; Mahon et al., 2013; Kristensen et al., 2016), a process that may be of critical importance in the face of conflicting use and grasp actions.

Finally, we showed that a model including both tissue integrity and functional connectivity predicted apraxic behavior better than when lesions alone were considered. Other recent studies have also highlighted the value in using multiple imaging modalities (e.g., diffusion tensor imaging, MRI) or measures (e.g., rs-fMRI) to improve predictions of patient performance (Hope et al., 2016; Kuceyeski et al., 2016; Siegel et al., 2016; Pustina et al., 2017). Additionally, we found that relative to VLSM, correlations between behavior and functional connectivity explained unique variance, even for left hemisphere voxels lesioned in sufficient numbers of subjects for VLSM analyses. This finding may reflect left hemisphere areas experiencing "connectional diaschisis", i.e., reduced connectivity with areas remote from the lesion (Carrera and Tononi, 2014), as well as abnormally-functioning peri-lesional tissue. The added ability to assess functional connectivity between hemispheres and within the intact right hemisphere, together with the ease of resting data collection in patient populations (Carter et al., 2012b), makes rs-fMRI an important complement to analyses based solely on lesion location.

Funding

This work was funded by NIH R01 NS099061 to Laurel J. Buxbaum, NIH AG017586 to Murray Grossman, and by NIH RO1 DC008779, NIH RO1 HD050199, and a NSF subcontract under SBE0541957 to Anjan Chatterjee. Stephen J. Gotts and Alex Martin were supported by the Intramural Research Program, National Institute of Mental Health (ZIAMH002920).

Acknowledgments

We thank H. Branch Coslett for overseeing the lesion segmentation and analysis process, Anjan Chatterjee and Murray Grossman for sharing their data from neurologically-intact participants, and Louisa Smith and Leyla Tarhan for their assistance in testing participants.

Appendix A. Supplementary data

Supplementary data to this article can be found online at https://doi.org/10.1016/j.nicl.2018.08.033.

References

Badre, D., Wagner, A.D., 2004. Selection, integration, and conflict monitoring: Assessing the nature and generality of prefrontal cognitive control mechanisms. Neuron 41, 473–487.
Baier, B., Karnath, H.-O., 2008. Tight link between our sense of limb ownership and self-awareness of actions. Stroke 39, 486–488.
Baldassarre, A., Ramsey, L., Hacker, C.L., Callejas, A., Astafiev, S.V., Metcalf, N.V., et al., 2014. Large-scale changes in network interactions as a physiological signature of spatial neglect. Brain 137, 3267–3283.
Baldassarre, A., Ramsey, L.E., Siegel, J.S., Shulman, G.L., Corbetta, M., 2016. Brain connectivity and neurological disorders after stroke. Curr. Opin. Neurol. 29, 706–713.
Barbieri, C., De Renzi, E., 1988. The executive and ideational components of apraxia. Cortex 24, 535–543.
Behzadi, Y., Restom, K., Liau, J., Liu, T.T., 2007. A component based noise correction method (CompCor) for BOLD and perfusion based fMRI. NeuroImage 37, 90–101.
Berman, R.A., Gotts, S.J., McAdams, H.M., Greenstein, D., Lalonde, F., Clasen, L., et al., 2016. Disrupted sensorimotor and social–cognitive networks underlie symptoms in childhood-onset schizophrenia. Brain 139, 276–291.
Binkofski, F., Buxbaum, L.J., 2013. Two action systems in the human brain. Brain Lang. 127, 222–229.
Bohlhalter, S., Hattori, N., Wheaton, L., Fridman, E., Shamim, E.A., Garraux, G., et al., 2009. Gesture subtype–dependent left lateralization of praxis planning: an event-related fMRI study. Cereb. Cortex 19, 1256–1262.
Botvinick, M.M., Braver, T.S., Barch, D.M., Carter, C.S., Cohen, J.D., 2001. Conflict monitoring and cognitive control. Psychol. Rev. 108, 624–652.
Brodeur, M.B., Dionne-Dostie, E., Montreuil, T., Lepage, M., 2010. The Bank of Standardized Stimuli (BOSS), a new set of 480 normative photos of objects to be used as visual stimuli in cognitive research. PLoS One 5, e10773.
Bullmore, E., Sporns, O., 2009. Complex brain networks: graph theoretical analysis of structural and functional systems. Nat. Rev. Neurosci. 10, 186–198.
Buxbaum, L.J., 2001. Ideomotor apraxia: a call to action. Neurocase 7, 44–458.
Buxbaum, L.J., 2017. Learning, remembering, and predicting how to use tools: distributed neurocognitive mechanisms: comment on Osiurak and Badets (2016). Psychol. Rev. 124, 346–360.
Buxbaum, L.J., Randerath, J., 2018 Jun 21. Limb apraxia and the left parietal lobe. In: Vallar, G, Coslett, H.B. (Eds.), Handbook of Clinical Neurology. Elsevier, pp. 349–363 [cited 2018 Jun 21].
Buxbaum, L.J., Sirigu, A., Schwartz, M.F., Klatzky, R.L., 2003. Cognitive representations of hand posture in ideomotor apraxia. Neuropsychologia 41, 1091–1113.
Buxbaum, L.J., Johnson-Frey, S.H., Bartlett-Williams, M., 2005a. Deficient internal models for planning hand–object interactions in apraxia. Neuropsychologia 43, 917–929.
Buxbaum, L.J., Kyle, K.M., Menon, R., 2005b. On beyond mirror neurons: Internal representations subserving imitation and recognition of skilled object-related actions in humans. Cogn. Brain Res. 25, 226–239.
Buxbaum, L.J., Kyle, K., Grossman, M., Coslett, H.B., 2007. Left inferior parietal representations for skilled hand-object interactions: evidence from stroke and corticobasal degeneration. Cortex 43, 411–423.
Buxbaum, L.J., Shapiro, A.D., Coslett, H.B., 2014. Critical brain regions for tool-related and imitative actions: a componential analysis. Brain 137, 1971–1985.
Carrera, E., Tononi, G., 2014. Diaschisis: past, present, future. Brain J. Neurol. 137, 2408–2422.
Carter, A.R., Astafiev, S.V., Lang, C.E., Connor, L.T., Rengachary, J., Strube, M.J., et al., 2010. Resting interhemispheric functional magnetic resonance imaging connectivity predicts performance after stroke. Ann. Neurol. 67, 365–375.
Carter, A.R., Patel, K.R., Astafiev, S.V., Snyder, A.Z., Rengachary, J., Strube, M.J., et al., 2012a. Upstream dysfunction of somatomotor functional connectivity after corticospinal damage in stroke. Neurorehabil. Neural Repair 26, 7–19.
Carter, A.R., Shulman, G.L., Corbetta, M., 2012b. Why use a connectivity-based approach to study stroke and recovery of function? NeuroImage 62, 2271–2280.

Chaminade, T., Meltzoff, A.N., Decety, J., 2005. An fMRI study of imitation: action representation and body schema. Neuropsychologia 43, 115–127.
Cole, M.W., Schneider, W., 2007. The cognitive control network: Integrated cortical regions with dissociable functions. NeuroImage 37, 343–360.
Cole, M.W., Pathak, S., Schneider, W., 2010. Identifying the brain's most globally connected regions. NeuroImage 49, 3132–3148.
Cox, R.W., 1996. AFNI: Software for analysis and visualization of functional magnetic resonance neuroimages. Comput. Biomed. Res. 29, 162–173.
Curtis, C.E., D'Esposito, M., 2003. Persistent activity in the prefrontal cortex during working memory. Trends Cogn. Sci. 7, 415–423.
De Renzi, E., Faglioni, P., Scarpa, M., Crisi, G., 1986. Limb apraxia in patients with damage confined to the left basal ganglia and thalamus. J. Neurol. Neurosurg. Psychiatry 49, 1030–1038.
Duncan, J., 2010. The multiple-demand (MD) system of the primate brain: mental programs for intelligent behaviour. Trends Cogn. Sci. 14, 172–179.
Eklund, A., Nichols, T.E., Knutsson, H., 2016. Cluster failure: why fMRI inferences for spatial extent have inflated false-positive rates. Proc. Natl. Acad. Sci. U. S. A. 113, 7900–7905.
van Elk, M., van Schie, H., Bekkering, H., 2014. The scope and limits of action semantics: Reply to comments on 'Action semantics: a unifying conceptual framework for the selective use of multimodal and modality-specific object knowledge'. Phys Life Rev 11, 273–279.
Farrer, C., Franck, N., Georgieff, N., Frith, C.D., Decety, J., Jeannerod, M., 2003. Modulating the experience of agency: a positron emission tomography study. NeuroImage 18, 324–333.
Fedorenko, E., Duncan, J., Kanwisher, N., 2013. Broad domain generality in focal regions of frontal and parietal cortex. Proc. Natl. Acad. Sci. U. S. A. 110, 16616–16621.
Fox, M.D., Greicius, M., 2010. Clinical applications of resting state functional connectivity. Front. Syst. Neurosci. 4, 19.
Fox, M.D., Raichle, M.E., 2007. Spontaneous fluctuations in brain activity observed with functional magnetic resonance imaging. Nat. Rev. Neurosci. 8, 700–711.
Gallivan, J.P., Chapman, C.S., McLean, D.A., Flanagan, J.R., Culham, J.C., 2013. Activity patterns in the category-selective occipitotemporal cortex predict upcoming motor actions. Eur. J. Neurosci. 38, 2408–2424.
Genovese, C.R., Lazar, N.A., Nichols, T., 2002. Thresholding of statistical maps in functional neuroimaging using the false discovery rate. NeuroImage 15, 870–878.
Goodale, M.A., Milner, A.D., 1992. Separate visual pathways for perception and action. Trends Neurosci. 15, 20–25.
Gotts, S.J., Simmons, W.K., Milbury, L.A., Wallace, G.L., Cox, R.W., Martin, A., 2012. Fractionation of social brain circuits in autism spectrum disorders. Brain 135, 2711–2725.
Gotts, S.J., Gilmore, A.W., Martin, A., 2018. Brain Networks, Dimensionality, and Global Signal Averaging in Resting-State fMRI: Hierarchical Network Structure Results in Low-Dimensional Spatiotemporal Dynamics.
Haaland, K.Y., Flaherty, D., 1984. The different types of limb apraxia errors made by patients with left vs. right hemisphere damage. Brain Cogn. 3, 370–384.
Haaland, K.Y., Harrington, D.L., Knight, R.T., 2000. Neural representations of skilled movement. Brain 123, 2306–2313.
Haber, S.N., Calzavara, R., 2009. The cortico-basal ganglia integrative network: the role of the thalamus. Brain Res. Bull. 78, 69–74.
Hahamy, A., Calhoun, V., Pearlson, G., Harel, M., Stern, N., Attar, F., et al., 2014. Save the global: global signal connectivity as a tool for studying clinical populations with functional magnetic resonance imaging. Brain Connect. 4, 395–403.
Hanna-Pladdy, B., Daniels, S.K., Fieselman, M.A., Thompson, K., Vasterling, J.J., Heilman, K.M., et al., 2001. Praxis lateralization: errors in right and left hemisphere stroke. Cortex J. Devoted Study Nerv. Syst. Behav. 37, 219–230.
Hayward, K.S., Neva, J.L., Mang, C.S., Peters, S., Wadden, K.P., Ferris, J.K., et al., 2017. Interhemispheric pathways are important for motor outcome in individuals with chronic and severe upper limb impairment post stroke. Neural Plast. 2017 (Article ID 4281532, 12 pages).
He, B.J., Snyder, A.Z., Vincent, J.L., Epstein, A., Shulman, G.L., Corbetta, M., 2007. Breakdown of functional connectivity in frontoparietal networks underlies behavioral deficits in spatial neglect. Neuron 53, 905–918.
Heath, M., Roy, E.A., Black, S.E., Westwood, D.A., 2001. Intransitive limb gestures and apraxia following unilateral stroke. J. Clin. Exp. Neuropsychol. 23, 628–642.
Hermsdörfer, J., Terlinden, G., Mühlau, M., Goldenberg, G., Wohlschläger, A.M., 2007. Neural representations of pantomimed and actual tool use: evidence from an event-related fMRI study. NeuroImage 36 (Supplement 2), T109–T118.
Hickok, G., Poeppel, D., 2004. Dorsal and ventral streams: a framework for understanding aspects of the functional anatomy of language. Cognition 92, 67–99.
Hickok, G., Poeppel, D., 2007. The cortical organization of speech processing. Nat. Rev. Neurosci. 8, 393–402.
Hickok, G., Bellugi, U., Klima, E.S., 1998. The neural organization of language: evidence from sign language aphasia. Trends Cogn. Sci. 2, 129–136.
Hoeren, M., Kümmerer, D., Bormann, T., Beume, L., Ludwig, V.M., Vry, M.-S., et al., 2014. Neural bases of imitation and pantomime in acute stroke patients: distinct streams for praxis. Brain 137, 2796–2810.
Hope, T.M.H., Seghier, M.L., Prejawa, S., Leff, A.P., Price, C.J., 2016. Distinguishing the effect of lesion load from tract disconnection in the arcuate and uncinate fasciculi. NeuroImage 125, 1169–1173.
Hwang, K., Bertolero, M.A., Liu, W.B., D'Esposito, M., 2017. The human thalamus is an integrative hub for functional brain networks. J. Neurosci. 37, 5594–5607.
Ishibashi, R., Pobric, G., Saito, S., Lambon Ralph, M.A., 2016. The neural network for tool-related cognition: an activation likelihood estimation meta-analysis of 70 neuroimaging contrasts. Cogn. Neuropsychol. 33, 241–256.
Jarry, C., Osiurak, F., Delafuys, D., Chauviré, V., Etcharry-Bouyx, F., Le Gall, D., 2013. Apraxia of tool use: more evidence for the technical reasoning hypothesis. Cortex 49, 2322–2333.
Jax, S.A., Buxbaum, L.J., 2010. Response interference between functional and structural actions linked to the same familiar object. Cognition 115, 350–355.
Jax, S.A., Buxbaum, L.J., 2013. Response interference between functional and structural object-related actions is increased in patients with ideomotor apraxia. J. Neuropsychol. 7, 12–18.
Jo, H.J., Saad, Z.S., Simmons, W.K., Milbury, L.A., Cox, R.W., 2010. Mapping sources of correlation in resting state FMRI, with artifact detection and removal. NeuroImage 52, 571–582.
Kalénine, S., Buxbaum, L.J., Coslett, H.B., 2010. Critical brain regions for action recognition: lesion symptom mapping in left hemisphere stroke. Brain 133, 3269–3280.
Kalénine, S., Wamain, Y., Decroix, J., Coello, Y., 2016. Conflict between object structural and functional affordances in peripersonal space. Cognition 155, 1–7.
Karnath, H.-O., Baier, B., Nägele, T., 2005. Awareness of the functioning of one's own limbs mediated by the insular cortex? J. Neurosci. 25, 7134–7138.
Kertesz, A., 1982. Western Aphasia Battery. Grune & Stratton, New York.
Kristensen, S., Garcea, F.E., Mahon, B.Z., Almeida, J., 2016. Temporal frequency tuning reveals interactions between the dorsal and ventral visual streams. J. Cogn. Neurosci. 28, 1295–1302.
Króliczak, G., Cavina-Pratesi, C., Goodman, D.A., Culham, J.C., 2007. What does the brain do when you fake it? An fMRI study of pantomimed and real grasping. J. Neurophysiol. 97, 2410–2422.
Króliczak, G., Piper, B.J., Frey, S.H., 2016. Specialization of the left supramarginal gyrus for hand-independent praxis representation is not related to hand dominance. Neuropsychologia 93, 501–512.
Kuceyeski, A., Navi, B.B., Kamel, H., Raj, A., Relkin, N., Toglia, J., et al., 2016. Structural connectome disruption at baseline predicts 6-months post-stroke outcome. Hum. Brain Mapp. 37, 2587–2601.
Lausberg, H., Cruz, R.F., Kita, S., Zaidel, E., Ptito, A., 2003. Pantomime to visual presentation of objects: left hand dyspraxia in patients with complete callosotomy. Brain 126, 343–360.
Lewis, J.W., 2006. Cortical networks related to human use of tools. Neuroscientist 12, 211–231.
MacDonald, A.W., Cohen, J.D., Stenger, V.A., Carter, C.S., 2000. Dissociating the role of the dorsolateral prefrontal and anterior cingulate cortex in cognitive control. Science 288, 1835–1838.
Mahon, B.Z., Kumar, N., Almeida, J., 2013. Spatial frequency tuning reveals interactions between the dorsal and ventral visual systems. J. Cogn. Neurosci. 25, 862–871.
Maris, E., Oostenveld, R., 2007. Nonparametric statistical testing of EEG- and MEG-data. J. Neurosci. Methods 164, 177–190.
Martin, A., Simmons, K.W., Beauchamp, M.S., Gotts, S.J., 2014. Is a single 'hub', with lots of spokes, an accurate description of the neural architecture of action semantics?: comment on 'Action semantics: a unifying conceptual framework for the selective use of multimodal and modality-specific object knowledge' by van Elk, van Schie and Bekkering. Phys Life Rev 11, 261–262.
Martin, M., Nitschke, K., Beume, L., Dressing, A., Bühler, L.E., Ludwig, V.M., et al., 2016. Brain activity underlying tool-related and imitative skills after major left hemisphere stroke. Brain 139, 1497–1516.
Meoded, A., Morrissette, A.E., Katipally, R., Schanz, O., Gotts, S.J., Floeter, M.K., 2015. Cerebro-cerebellar connectivity is increased in primary lateral sclerosis. NeuroImage Clin. 7, 288.
Miller, E.K., Cohen, J.D., 2001. An integrative theory of prefrontal cortex function. Annu. Rev. Neurosci. 24, 167–202.
Milner, A.D., Goodale, M.A., 2008. Two visual systems re-viewed. Neuropsychologia 46, 774–785.
Nadeau, S.E., Roeltgen, D.P., Sevush, S., Ballinger, W.E., Watson, R.T., 1994. Apraxia due to a pathologically documented thalamic infarction. Neurology 44, 2133.
Noonan, K.A., Jefferies, E., Visser, M., Lambon Ralph, M.A., 2013. Going beyond inferior prefrontal involvement in semantic control: evidence for the additional contribution of dorsal angular gyrus and posterior middle temporal cortex. J. Cogn. Neurosci. 25, 1824–1850.
Orban, G.A., Caruana, F., 2014. The neural basis of human tool use. Front. Psychol. 5, 310.
Ovadia-Caro, S., Margulies, D.S., Villringer, A., 2014. The value of resting-state functional magnetic resonance imaging in stroke. Stroke 45, 2818–2824.
Power, J.D., Barnes, K.A., Snyder, A.Z., Schlaggar, B.L., Petersen, S.E., 2012. Spurious but systematic correlations in functional connectivity MRI networks arise from subject motion. NeuroImage 59, 2142–2154.
Power, J.D., Schlaggar, B.L., Petersen, S.E., 2014. Studying brain organization via spontaneous fMRI signal. Neuron 84, 681–696.
Pustina, D., Coslett, H.B., Ungar, L., Faseyitan, O.K., Medaglia, J.D., Avants, B., et al., 2017. Enhanced estimations of post-stroke aphasia severity using stacked multimodal predictions. Hum. Brain Mapp. 38, 5603–5615.
Randerath, J., Goldenberg, G., Spijkers, W., Li, Y., Hermsdörfer, J., 2010. Different left brain regions are essential for grasping a tool compared with its subsequent use. NeuroImage 53, 171–180.
Rizzolatti, G., Matelli, M., 2003. Two different streams form the dorsal visual system: anatomy and functions. Exp. Brain Res. 153, 146–157.
Roy, E.A., Heath, M., Westwood, D., Schweizer, T.A., Dixon, M.J., Black, S.E., et al., 2000. Task demands and limb apraxia in stroke. Brain Cogn. 44, 253–279.
Saad, Z.S., Reynolds, R.C., Jo, H.J., Gotts, S.J., Chen, G., Martin, A., et al., 2013. Correcting brain-wide correlation differences in resting-state fMRI. Brain Connect. 3, 339–352.
Sakreida, K., Effnert, I., Thill, S., Menz, M.M., Jirak, D., Eickhoff, C.R., et al., 2016. Affordance processing in segregated parieto-frontal dorsal stream sub-pathways.

Neurosci. Biobehav. Rev. 69, 89–112.
Salomon, R., Bleich-Cohen, M., Hahamy-Dubossarsky, A., Dinstien, I., Weizman, R., Poyurovsky, M., et al., 2011. Global functional connectivity deficits in schizophrenia depend on behavioral state. J. Neurosci. 31, 12972–12981.
Saur, D., Kreher, B.W., Schnell, S., Kümmerer, D., Kellmeyer, P., Vry, M.-S., et al., 2008. Ventral and dorsal pathways for language. Proc. Natl. Acad. Sci. U. S. A. 105, 18035–18040.
Schwartz, M.F., Brecher, A.R., Whyte, J., Klein, M.G., 2005. A patient registry for cognitive rehabilitation research: a strategy for balancing patients' privacy rights with researchers' need for access. Arch. Phys. Med. Rehabil. 86, 1807–1814.
Siegel, J.S., Ramsey, L.E., Snyder, A.Z., Metcalf, N.V., Chacko, R.V., Weinberger, K., et al., 2016. Disruptions of network connectivity predict impairment in multiple behavioral domains after stroke. Proc. Natl. Acad. Sci. U. S. A. 113, E4367–E4376.
Siegel, J.S., Shulman, G.L., Corbetta, M., 2017. Measuring functional connectivity in stroke: Approaches and considerations. J. Cereb. Blood Flow Metab. 37, 2665–2678.
Song, S., Gotts, S.J., Dayan, E., Cohen, L.G., 2015. Practice structure improves unconscious transitional memories by increasing synchrony in a premotor network. J. Cogn. Neurosci. 27, 1503–1512.
Stamenova, V., Roy, E.A., Black, S.E., 2010. Associations and dissociations of transitive and intransitive gestures in left and right hemisphere stroke patients. Brain Cogn. 72, 483–490.
Stoddard, J., Gotts, S.J., Brotman, M.A., Lever, S., Hsu, D., Zarate, C., et al., 2016. Aberrant intrinsic functional connectivity within and between corticostriatal and temporal–parietal networks in adults and youth with bipolar disorder. Psychol. Med. 46, 1509–1522.
Tarhan, L.Y., Watson, C.E., Buxbaum, L.J., 2015. Shared and distinct neuroanatomic regions critical for tool-related action production and recognition: evidence from 131 left-hemisphere stroke patients. J. Cogn. Neurosci. 27, 2491–2511.
Urbin, M.A., Hong, X., Lang, C.E., Carter, A.R., 2014. Resting-state functional connectivity and its association with multiple domains of upper-extremity function in chronic stroke. Neurorehabil. Neural Repair 28, 761–769.
Vingerhoets, G., Vandekerckhove, E., Honoré, P., Vandemaele, P., Achten, E., 2011. Neural correlates of pantomiming familiar and unfamiliar tools: Action semantics versus mechanical problem solving? Hum. Brain Mapp. 32, 905–918.
Vry, M.-S., Tritschler, L.C., Hamzei, F., Rijntjes, M., Kaller, C.P., Hoeren, M., et al., 2015. The ventral fiber pathway for pantomime of object use. NeuroImage 106, 252–263.
Wamain, Y., Sahaï, A., Decroix, J., Coello, Y., Kalénine, S., 2018. Conflict between gesture representations extinguishes μ rhythm desynchronization during manipulable object perception: an EEG study. Biol. Psychol. 132, 202–211.
Watson, C.E., Buxbaum, L.J., 2015. A distributed network critical for selecting among tool-directed actions. Cortex 65, 65–82.
Watson, C.E., Cardillo, E.R., Ianni, G.R., Chatterjee, A., 2013. Action concepts in the brain: an activation likelihood estimation meta-analysis. J. Cogn. Neurosci. 25, 1191–1205.
Weiss, P.H., Ubben, S.D., Kaesberg, S., Kalbe, E., Kessler, J., Liebig, T., et al., 2016. Where language meets meaningful action: a combined behavior and lesion analysis of aphasia and apraxia. Brain Struct. Funct. 221, 563–576.
Xu, J., Gannon, P.J., Emmorey, K., Smith, J.F., Braun, A.R., 2009. Symbolic gestures and spoken language are processed by a common neural system. Proc. Natl. Acad. Sci. 106, 20664–20669.
Xu, H., Qin, W., Chen, H., Jiang, L., Li, K., Yu, C., 2014. Contribution of the resting-state functional connectivity of the contralesional primary sensorimotor cortex to motor recovery after subcortical stroke. PLoS One 9, e84729.